

Direct signatures of Anderson orthogonality catastrophe in nonequilibrium quantum dots

Sarath Sankar,^{1,*} Joshua Folk,^{2,3} Yigal Meir,⁴ and Eran Sela¹

¹*School of Physics and Astronomy, Tel Aviv University, Tel Aviv 6997801, Israel*

²*Quantum Matter Institute, University of British Columbia, Vancouver, British Columbia, Canada*

³*Department of Physics and Astronomy, University of British Columbia, Vancouver, British Columbia, Canada*

⁴*Department of Physics, Ben-Gurion University of the Negev, Beer-Sheva 84105, Israel*

(Dated: July 8, 2025)

We propose schemes for unambiguous direct observation of Anderson orthogonality catastrophe (AOC) effects in a quantum dot coupled to a charge detector, and to estimate the strength of the AOC exponent α . We show that certain easy-to-measure observables have a robust dependence on α in the non-equilibrium regimes of source-drain voltage bias or thermal imbalance. Our results are obtained using a rate equation formalism in which the AOC effects on tunnel rates are incorporated in an exact manner.

I. INTRODUCTION

The Anderson orthogonality catastrophe (AOC) occurs due to the response of a Fermi sea to a sudden change in local potential¹. It is characterized by a universal exponent α describing the power-law decay of the overlap of the perturbed and unperturbed many-body ground state in the thermodynamic limit $L \rightarrow \infty$, $\langle GS|GS' \rangle \propto 1/L^\alpha$. A family of systems in which the AOC has been claimed to be relevant are quantum dots (QDs) capacitively coupled to a charge detector; the detector Fermi sea is affected by the charge state of the QD and AOC arises when tunnel events occur in the QD.

The AOC in the detector manifests as measurement back action²⁻⁴ on the physical observables of the QD. When strong enough, AOC can drive phase transitions^{5,6}. The AOC exponent in general also receives additional contributions from interactions of the QD with its lead⁷ (as in the interacting resonant level model), with other localized levels⁸, or with other nearby gates. Yet, an unambiguous experimental observation of AOC effects, including the determination of α , in QDs coupled to detectors remains elusive. This is mainly because of the presence of other dominant mechanisms contributing to back action, such as dephasing which for example can arise due to the current noise in the detector. In fact almost all of the reported experimental observations of back action effects in QDs are attributed to such dephasing phenomenon⁹⁻¹³.

Here we show that in a weakly tunnel coupled QD that is driven strongly out of equilibrium, the AOC signatures controlled by α can be isolated from other back action effects like dephasing. We consider two kinds of non-equilibrium in the QD: (i) source drain voltage V across the QD leads (see Fig. 1(a)), and (ii) different temperatures in the QD leads and detector (see Fig. 4(a)). In both the cases we identify direct approaches to experimentally measure α from the back action signatures on the QD observables such as its charge curve or steady state current.

II. MODEL

We consider the same model of Ref. 3, with $H = H_{\text{sys}} + H_{\text{det}} + H_\lambda$. The system consists of a spinless QD with energy ϵ_d tunnel coupled to L and R leads with tunneling coupling $\Gamma_{L/R}$. We consider two charge states of the QD denoted $n = 0, 1$. In this paper we only consider the limit of weak tunneling in the QD, $\Gamma_{L,R} \ll T$, and hybridization effects are neglected. The detector consists of another quantum dot (QDD). Its Hamiltonian including its coupling with the system's QD depends on n , and is described by $H_n = H_{\text{det}} + H_\lambda$ with

$$H_n = \sum_{i=1}^m [\epsilon_d d_i^\dagger d_i + \sum_{\mu=L,R} (\epsilon_k \varphi_{ki\mu}^\dagger \varphi_{ki\mu} + v_\mu \varphi_{ki\mu}^\dagger d_i + h.c.)] + \lambda \sum_{i=1}^m \left(d_i^\dagger d_i - \frac{1}{2} \right) \left(n - \frac{1}{2} \right), \quad (1)$$

where d_i^\dagger creates an electron in the QDD, and $\varphi_{ki\mu}^\dagger$ creates an electron with momentum k in detector lead μ . Here i denotes additional indices (like spin) which for simplicity we treat as a degeneracy factor m . The total tunneling width of the QDD is $\Gamma_q = 2\pi\nu_d(v_L^2 + v_R^2)$. The tunneling in the QDD is assumed to be strong, $\Gamma_q \gg T$.

In this model we control the AOC exponent α via m and λ , as $\alpha = m(\delta/\pi)^2$ where

$$\delta = \arctan\left(\frac{\epsilon_q + \lambda/2}{\Gamma_q}\right) - \arctan\left(\frac{\epsilon_q - \lambda/2}{\Gamma_q}\right). \quad (2)$$

A. Tunneling rates

As discussed in Ref. 3, in the presence of the capacitive coupling to the detector, the tunnel rates of the system QD from/to the lead $i = L/R$ are given by

$$\Gamma_i^{\text{in}} = \Gamma_i \int dE f(E - \mu_i) A^+(E - \epsilon_d), \quad (3)$$

$$\Gamma_i^{\text{out}} = \Gamma_i \int dE (1 - f(E - \mu_i)) A^-(E - \epsilon_d), \quad (4)$$

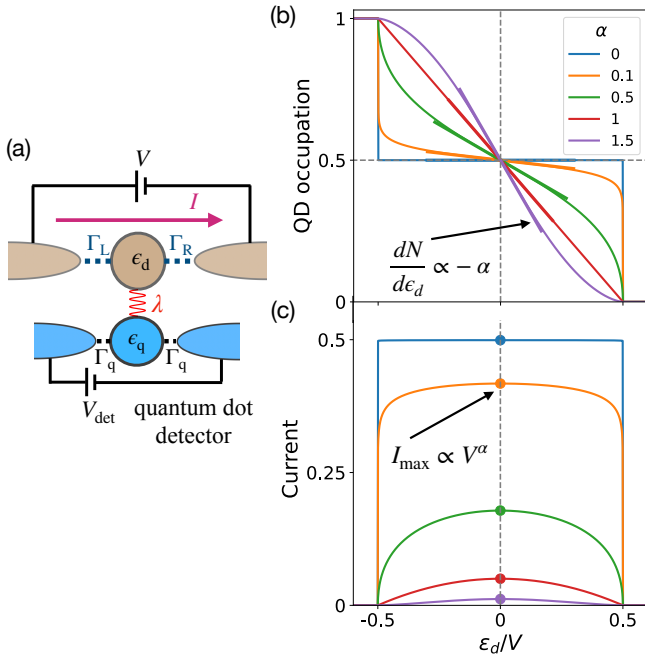


FIG. 1: (a) Schematic of a QD weakly tunnel coupled ($\Gamma_{L,R}$) to voltage biased leads, and capacitively coupled (λ) to a quantum dot detector. α is a dimensionless exponent associated with the Anderson orthogonality catastrophe in the detector due to tunnel events in the QD. Panels (b), (c) discuss the spinless case of the QD with $\Gamma_L = \Gamma_R = \Gamma$ and the limit $T, V_{det} \rightarrow 0$. (b) Average occupation of the QD, $N(\epsilon_d)$, and the average steady state current, $I(\epsilon_d)$, depends strongly on α in the energy window $\epsilon_d \in [-V/2, V/2]$ as shown respectively in (b) and (c). The slope of the bold lines in (b) gives the charge susceptibility that obeys $\partial N/\partial \epsilon_d|_{\epsilon_d=0} \propto -\alpha$, and provides a direct measure of α - see Eq. (17). The current peak (thick dots) in (c) that occurs at $\epsilon_d = 0$ is proportional to V^α and provides another direct measure of α - see Eq. (21).

where $f(E) = \frac{1}{e^{E/T} + 1}$ is the Fermi function and $A^{\pm}(E)$ are Fourier transforms of the corresponding functions defined in the time domain as,

$$A^{\pm}(t) = \text{Tr} [\rho_{0/1} e^{itH_0} e^{-itH_1}], \quad (5)$$

with $\rho_n \propto e^{-H_n/T}$ denoting the detector density matrix for QD charge n . The functions $A^\pm(E)$ are the key objects that incorporate the AOC. For their detailed calculation, see Ref. 3 and references therein. Particularly at $V_{det} = 0$ we have²

$$A^\pm(t) = \left(\frac{\pi T}{\pm i D \sinh(\pi T t)} \right)^\alpha, \quad (t \gg 1/D), \quad (6)$$

where D denotes a high energy cutoff associated with the detector bandwidth; $D \sim \Gamma_q$ for our QDD. The Fourier transform of $A^\pm(t)$ is,

$$A^\pm(E) = \frac{\chi}{D} \left(\frac{T}{D} \right)^{\alpha-1} \text{Re} \left[\frac{e^{\pm i\pi\alpha/2} \Gamma \left(\frac{iE}{2\pi T} + \frac{\alpha}{2} \right)}{\Gamma \left(1 + \frac{iE}{2\pi T} - \frac{\alpha}{2} \right)} \right], \quad (7)$$

where χ is a nonuniversal prefactor³. Their zero temperature limit is

$$A^\pm(E) = \theta(\pm E) A |E|^{\alpha-1}, \quad (8)$$

with $A = \frac{\chi}{D^\alpha}$.

III. AOC SIGNATURES IN QD WITH VOLTAGE BIASED LEADS

We consider the non-equilibrium situation due to a source-drain voltage bias on the QD, with the leads held at chemical potentials $\mu_{L/R} = \pm eV/2$ (see Fig. 1(a)). While the system is driven out of equilibrium, the detector is taken to be essentially at equilibrium, i.e. $V_{det} \rightarrow 0$. We now identify direct manifestations of α in the non-equilibrium behavior of the QD when $V \gg T$.

A. Average occupation

The average QD occupation N is governed by the rate equation

$$\frac{dN}{dt} = (1 - N)[\Gamma_L^{\text{in}} + \Gamma_R^{\text{in}}] - N[\Gamma_L^{\text{out}} + \Gamma_R^{\text{out}}]. \quad (9)$$

At steady state we get

$$N = \frac{\Gamma_L^{\text{in}} + \Gamma_R^{\text{in}}}{\Gamma_L^{\text{in}} + \Gamma_R^{\text{in}} + \Gamma_L^{\text{out}} + \Gamma_R^{\text{out}}}. \quad (10)$$

At equilibrium, $V = V_{det} = 0$, the average occupation becomes a Fermi function, $N = f(\epsilon_d - \Delta)$, with Δ being a constant energy shift independent of ϵ_d . This follows from the relation

$$A^-(E) = e^{-\beta(E+\Delta)} A^+(E), \quad (11)$$

where $\Delta = F_{det}(1) - F_{det}(0)$, with $F_{det}(n)$ denoting the free energy of the detector for the system QD charge state n . Thus the charge curve, N versus ϵ_d , is not affected by α when $V = 0$ except for the effective shift of ϵ_d which we ignore from here on.

Now let us discuss the case $V \neq 0$ but consider the limit $T, V_{det} \rightarrow 0$. In this limit from Eqs. (8) we have

$$\Gamma_i^{\text{in}}(\epsilon_d) \stackrel{T \rightarrow 0}{=} \theta(\mu_i - \epsilon_d) \frac{A \Gamma_i}{\alpha} (\mu_i - \epsilon_d)^\alpha, \quad (12)$$

$$\Gamma_i^{\text{out}}(\epsilon_d) \stackrel{T \rightarrow 0}{=} \theta(\epsilon_d - \mu_i) \frac{A \Gamma_i}{\alpha} (\epsilon_d - \mu_i)^\alpha. \quad (13)$$

Thus the tunnel rates show a power-law dependence on the distance of the non-equilibrium chemical potentials $\mu_{L/R}$ from the level ϵ_d . Plugging these tunnel rates in Eq. (10) with $\mu_{L/R} = \pm V/2$ yields, $N(\epsilon_d < -V/2) = 1$, $N(\epsilon_d > V/2) = 0$, and for $V/2 < \epsilon_d < V/2$ we have $N = \frac{\Gamma_L^{\text{in}}}{\Gamma_L^{\text{in}} + \Gamma_R^{\text{out}}}$, giving

$$N \stackrel{T \rightarrow 0}{=} \frac{\Gamma_L (\frac{V}{2} - \epsilon_d)^\alpha}{\Gamma_L (\frac{V}{2} - \epsilon_d)^\alpha + \Gamma_R (\frac{V}{2} + \epsilon_d)^\alpha} \quad (-V/2 < \epsilon_d < V/2). \quad (14)$$

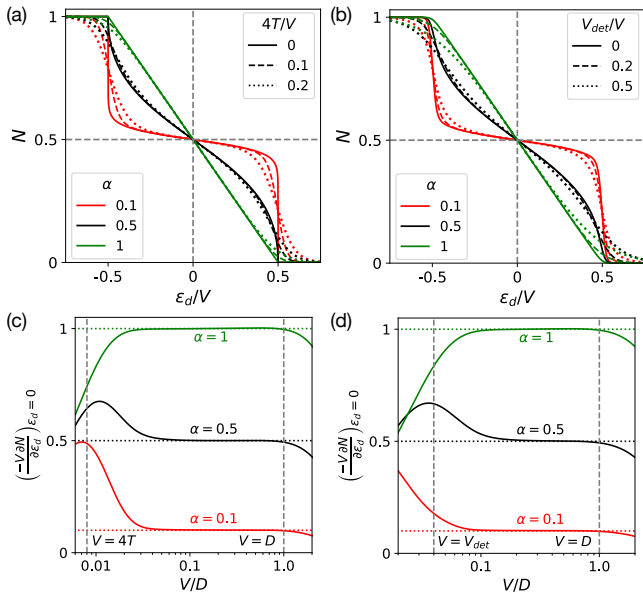


FIG. 2: Effect of (a) finite temperature and (b) detector bias on the average occupation of the QD in presence of α . Here the symmetric case $\Gamma_L = \Gamma_R$ is considered. For $V \gg T, V_{det}$ the two charge steps gets modified however the middle region ($\epsilon_d \approx 0$) is nearly unaffected. (c,d): The charge susceptibility at $\epsilon_d = 0$ remains a robust measure of α even in the presence of temperature and detector bias in the regime $T, V_{det} \ll V < D$, with $D \sim \Gamma_q$ being the high energy cutoff associated with the detector.

This is plotted in Fig. 1(b) for different values of α . The charge plateau for $\alpha = 0$ that occurs for $-V/2 < \epsilon_d < V/2$ is clearly modified by a finite α . Interestingly, the average occupation at the center of the step $\epsilon_d = \frac{\mu_L + \mu_R}{2} = 0$, for any asymmetry Γ_L/Γ_R , is not affected by α ,

$$N_c \equiv N(\epsilon_d = 0) = \frac{\Gamma_L}{\Gamma_L + \Gamma_R}, \quad (15)$$

while the slope, i.e. charge susceptibility at that point, is given by

$$\left(\frac{\partial N}{\partial \epsilon_d}\right)_{\epsilon_d=0} = \frac{-4\alpha\Gamma_L\Gamma_R}{V(\Gamma_L + \Gamma_R)^2}. \quad (16)$$

Using Eq. (15) we then obtain a simple relation connecting the charge susceptibility to α ,

$$\alpha = \frac{-V}{4N_c(1 - N_c)} \left(\frac{\partial N}{\partial \epsilon_d}\right)_{\epsilon_d=0}. \quad (17)$$

This relation is convenient for experimentally inferring α since it is expressed in terms of quantities that are easy to measure and does not require the knowledge of parameters like $\Gamma_{L,R}$ or the lever arm.

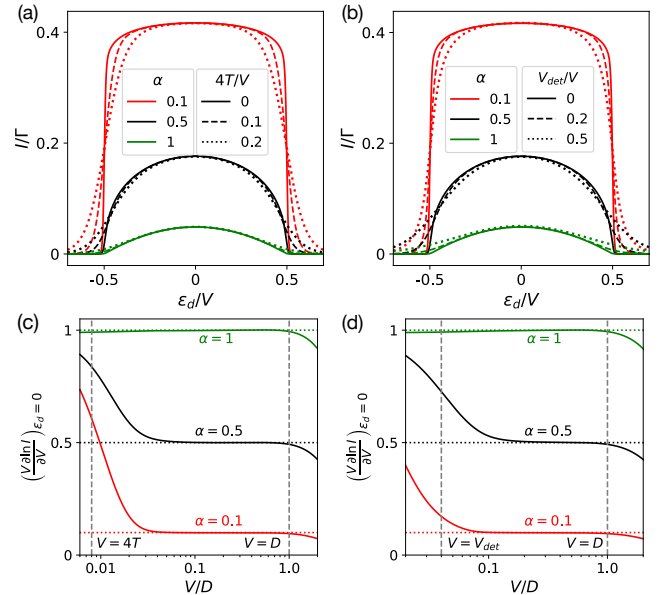


FIG. 3: Same as Fig. 2 but for the steady state current I . The voltage dependence of the current peak at $\epsilon_d = 0$ remains a robust measure of α in the regime $T, V_{det} \ll V < D$.

B. Steady state current

The steady state current from L to R is given (as either evaluated in the left or right tunnel junction),

$$I = (1 - N)\Gamma_L^{\text{in}} - N\Gamma_L^{\text{out}} = N\Gamma_R^{\text{out}} - (1 - N)\Gamma_R^{\text{in}}. \quad (18)$$

Plugging the expression for tunnel rates in Eqs. (12), (13) and for N in Eq. (14), we first see that $I(\epsilon_d < \mu_L) = I(\epsilon_d > \mu_R) = 0$. (Note that we focus only on the sequential tunneling current since we are actually interested in the regime $\epsilon_d \sim \frac{\mu_L + \mu_R}{2}$ and ignore the cotunneling current) Next, for the QD level in-between the two chemical potentials, we get,

$$I(\epsilon_d) \stackrel{T \rightarrow 0}{=} \frac{\frac{A}{\alpha}\Gamma_L\Gamma_R \left(\left(\frac{V}{2}\right)^2 - \epsilon_d^2\right)^\alpha}{\Gamma_L\left(\frac{V}{2} - \epsilon_d\right)^\alpha + \Gamma_R\left(\frac{V}{2} + \epsilon_d\right)^\alpha}, \quad \left(|\epsilon_d| < \frac{V}{2}\right), \quad (19)$$

This is plotted in Fig. 1(c) for different values of α . The current peaks at the mid-point between the two chemical potentials i.e. at $\epsilon_d = 0$ (independent of the asymmetry Γ_L/Γ_R), where it is given by

$$I(\epsilon_d = 0) \stackrel{T \rightarrow 0}{=} \frac{A}{\alpha} \frac{\Gamma_L\Gamma_R}{2^\alpha \Gamma_L + \Gamma_R} V^\alpha. \quad (20)$$

We clarify that this is derived in the sequential tunneling limit of small $\Gamma_{L,R}$, and indeed in this limit when $\alpha = 0$ the current for $\frac{V}{2} > |\epsilon_d|$ becomes independent of V as $T \rightarrow 0$. Interestingly when α is finite, the current shows a power law dependence on V : $I \propto V^\alpha$. Such power laws in the I-V characteristics appeared for example in transport through quantum point contacts in the

fractional quantum Hall regime or in Luttinger liquids¹⁴; here the exponent originates from the AOC. Thus α can be inferred from the V dependence of the peak,

$$\alpha = \frac{\partial \ln[I(\epsilon_d = 0)]}{\partial \ln V}. \quad (21)$$

This relation is convenient for experimentally inferring α as it only requires measuring the V -dependence of the peak current.

Equations (17) and (21) that relate α to two different observables of the system QD are the main results of this paper. We recall that these equations were derived under the assumptions of (i) the detector is at thermal equilibrium ($V_{det} = 0$) (ii) $T \rightarrow 0$.

C. Robustness at finite T and V_{det}

In this section we show that Eqs. (17) and Eq. (21) remain valid in the presence of a finite detector bias, V_{det} and finite T , provided that

$$\{T, V_{det}\} \ll V < D. \quad (22)$$

Note that a finite detector bias is required for experimentally measuring the QD occupation.

We follow Ref. 3 and compute the functions A^\pm at finite T and V_{det} using an exact numerical method generalizing the Nozierés-De Dominicis's solution¹⁵. Fig. 2 (a), (b) respectively shows the effect of finite T and V_{det} on $N(\epsilon_d)$. Their counterparts for $I(\epsilon_d)$ are shown respectively in Fig. 3 (a), (b). While we display in these figures only the value of α , in our calculation, the detector parameters are set at $\epsilon_q = 0$, $\Gamma_q = 1$ and m and λ are varied to obtain different α (for instance, $\lambda = 1.1$ and $m = 2$ for the case $\alpha = 0.2$). We remark that in the regime given by Eq. (22), the results in Figures 2 and 3 depend only on α and not on the specific detector parameters.

Let us focus on Fig. 2 (a). Consider first the two steps of the charge curve at $\epsilon_d = \mu_{L/R}$. These steps display power-law behavior, for example near $\epsilon_d \rightarrow V/2$ we have at $T = V_{det} = 0$ that $N \sim (V/2 - \epsilon_d)^\alpha$. We can see that these power law steps are thermally smeared by finite T . On the other hand, as long as $T \ll V$, the behavior near the middle of the plateau $\epsilon_d = 0$ remains nearly unaffected by temperature and retains its power-law behavior $dN/dT \propto -\alpha$. As shown in Fig. 2 (c), this allows to extract α using Eq. (17) in the regime given by Eq. (22). The high V limitation in Eq. (22) stems from the fact that the power-law regime of the detector functions $A^\pm(E)$ is limited to a finite energy range dictated by the detector band-width $D = \Gamma_q$.

The dependence on the detector bias is more involved, since in addition to supplying energy to the system, the AOC itself is modified in the non-equilibrium detector when there are multiple coupled Fermi edges^{16–18}. Nevertheless, a somewhat similar behavior occurs at finite V_{det} as compared to finite T , see Fig. 2 (b). Like in the

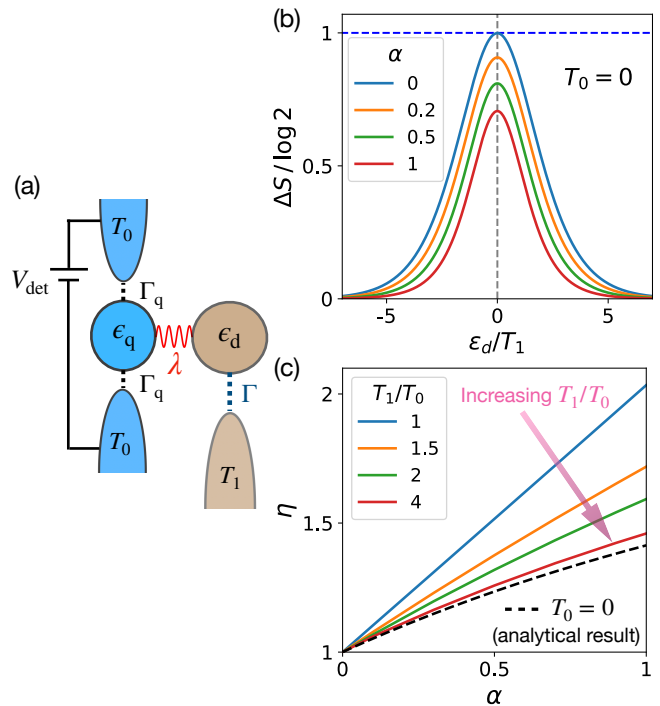


FIG. 4: (a) The schematic of the setup with different temperatures in the detector (T_0) and QD lead (T_1). (b) The “entropy change” of the QD calculated using Eq. 25. Here the case $T_0 = 0$ is considered (T_1 is arbitrary). The entropy peak at $\epsilon_d = 0$, S_{max} , decreases with α reflecting the violation of the thermodynamic Maxwell relation due to thermal imbalance; the ratio $\eta = \log 2/S_{max}$ provides a direct measure of α and is shown in (c) as dashed lines. (c) η for finite T_0 and T_1 increases monotonically with α . Here $T_0 = 0.03D$. η converges to the analytic result for $T_0 = 0$ as the ratio T_1/T_0 increases.

finite T case, we can apply Eq. (17) in the regime Eq. (22) to extract α as shown in Fig. 2 (d).

The above considerations also apply for the steady state current. This is shown in Fig. 3. Specifically, Fig. 3 (a), (b) show that in the regime Eq. (22), the current peak is nearly unaffected due to a finite T or V_{det} ; α can then be reliably extracted using Eq. (21) as shown in Fig. 3 (c), (d)

IV. AOC SIGNATURES IN THERMAL IMBALANCE

We now consider another kind of non-equilibrium: the QD leads are at temperature T_1 and charge detector at temperature T_0 with $T_1 \neq T_0$, and we set $V = V_{det} = 0$. Here it is sufficient to consider a single QD lead with tunnel coupling $\Gamma = \Gamma_L + \Gamma_R$, as shown in Fig. 4(a). The thermal imbalance will affect the QD observables such as N which is no longer given by a Fermi function, and the strength of the affect will depend on α . We discuss a possible way to properly quantify the thermal

imbalance associated with α , and thereby propose a route to measure α in experiments.

Let us first consider the case with $T_0 = 0$ and finite T_1 . Plugging Eq. (8) in the expression for the tunnel rates in Eq. (3) and Eq. (4), we get,

$$\Gamma_{\text{in/out}} = -\Gamma A T_1^\alpha \text{Li}_\alpha(-e^{\mp x}), \quad (23)$$

where $x = \epsilon_d/T_1$ and Li_α is the polylogarithm function of order α . The average occupation in steady state then follows from Eq. (10),

$$N(x; \alpha) = \frac{1}{1 + \text{Li}_\alpha(-e^x)/\text{Li}_\alpha(-e^{-x})}. \quad (24)$$

Note that when $\alpha = 0$, the expression reduces to the Fermi function, $N = 1/(1 + e^x)$. Finite α modifies N and in particular the width of the charge curve reduces with α .

The thermal imbalance associated with α can be quantified by the degree of violation of some thermodynamic relation. We consider the violation of the Maxwell relation, $\partial S/\partial \epsilon_d = -\partial N/\partial T_1$, where S denotes the thermodynamic entropy of the system. In particular, we consider the entropy change by integrating the Maxwell relation,

$$\Delta S(\epsilon_d) = \int_{\epsilon_d}^{\infty} \frac{\partial N}{\partial T_1} \Big|_{\epsilon'_d} d\epsilon'_d. \quad (25)$$

We remark that such Maxwell relation based entropy measurements have recently attracted experimental ¹⁹⁻²¹ and theoretical attention ²²⁻³¹. Taking the entropy of the empty QD (i.e $\epsilon_d \rightarrow \infty$) to be 0, we define the maximum entropy, $S_{\text{max}} = \Delta S(\epsilon_d = 0)$. Note that for $\alpha = 0$, the Maxwell relation is obeyed and we have $S_{\text{max}} = \log 2$, reflecting the degeneracy of the empty and occupied QD states at $\epsilon_d = 0$. But for finite α the Maxwell relation is violated by an amount which increases with α , see Fig. 4(b). We define,

$$\eta(\alpha) = \frac{\log 2}{S_{\text{max}}(\alpha)}, \quad (26)$$

which is a measure of the thermal imbalance associated with α . For the case $T_0 = 0$ we have,

$$S_{\text{max}}(\alpha) \stackrel{T_0=0}{=} - \int_0^{\infty} dx x \frac{\partial N(x; \alpha)}{\partial x} = \int_0^{\infty} dx N(x; \alpha). \quad (27)$$

Plugging in Eq. (24), we then have an analytic expression for $\eta(\alpha)$ at $T_0 = 0$. This is plotted as dashed lines in Fig. 4(c).

For finite T_0 , the thermal imbalance becomes a function of both T_0 and α and so does $\eta(\alpha)$. Fig. 4(c) shows $\eta(\alpha)$ for a fixed $T_0 = 0.03D$ and different T_1 . We find that as the ratio T_1/T_0 increases, the corresponding $\eta(\alpha)$ converges to the result for $T_0 = 0$. Thus, similar to the voltage biased case, a strong non-equilibrium condition

due to thermal imbalance allows for a reliable estimation of α in the regime:

$$T_0 \ll T_1 < D. \quad (28)$$

The proposed scheme to measure α works for finite V_{det} as well, provided the dephasing rate³, $\Gamma_\varphi(V_{\text{det}}) \ll T_1$.

V. GENERALIZATIONS

Although we considered a particular model, the key results are more general in the following sense. The AOC exponent α can stem from multiple electrostatically coupled metals or gates nearby to the QD. The power-law form of $A^\pm(E)$ is universal, and the value of α is additive as long as these various metals do not interact with each other. Indeed, in this case the functions $A^\pm(E)$ become products over these different metals. This factorization follows from the definition Eq. 5. Similarly, the detector does not have to be a QDD.

Secondly, we considered a spinless QD. This allows for the simplest way to directly detect α by applying a large Zeeman field. However in the presence of spin the analysis is only slightly modified as we now outline.

To include spin, consider the Anderson model

$$H_{\text{sys}} = \sum_{\sigma} \epsilon_d d_{\sigma}^{\dagger} d_{\sigma} + U d_{\uparrow}^{\dagger} d_{\uparrow} d_{\downarrow}^{\dagger} d_{\downarrow} + \sum_{ik\sigma} \epsilon_k c_{ik\sigma}^{\dagger} c_{ik\sigma} + \sum_{ik\sigma} \left(\gamma_i c_{ik\sigma}^{\dagger} d_{\sigma} + \text{H.c.} \right). \quad (29)$$

Here, d_{σ}^{\dagger} creates an electron in QD with spin σ and energy ϵ_d , and U is the onsite interaction. The QD number operator is $\hat{N} = \sum_{\sigma} d_{\sigma}^{\dagger} d_{\sigma}$. The left/right leads are labeled by $i \in \{L, R\}$ and $c_{ik\sigma}^{\dagger}$ creates an electron in the lead i with spin σ and energy ϵ_k . We assume the wide-band limit in the leads with a constant density of states (DoS) ν_i , resulting in energy-independent line widths, $\Gamma_i = 2\pi\nu_i|\gamma_i|^2$.

First consider the schemes discussed for the case of voltage biased QD in Sec. III. As a function of increasing ϵ_d , at $T = V = 0$ there are two charge steps, at $\epsilon_d = -U$ from $n = 2$ to $n = 1$ and then at $\epsilon_d = 0$ from $n = 1$ to $n = 0$. Let us push U to large values and focus on the $n = 0 \rightarrow 1$ charge step as before. Upon turning on V this single step splits into two steps at $\pm V/2$ as in Fig. 1(b). The only difference in the rate equations is that the tunnel-in rates contain an extra factor of 2 due to spin degeneracy as compared to the tunnel-out rates. As a result, Eq. (14) obtains the simple modification $\Gamma_L^{(in)} \rightarrow 2\Gamma_L^{(in)}$. A similar change occurs in Eq. (19). Thus our results in Sec. III will apply with minor modifications in the spinful case provided that $V \ll U$. A similar consideration applies to the scheme discussed for the thermal imbalance case in Sec. IV, and the results there will apply with minor modifications in the spinful case provided that $T_1 \ll U$.

VI. SUMMARY

In summary, we discussed simple schemes involving easy-to-measure observables in non-equilibrium conditions, such as the average charge or steady state current, to extract α for a QD capacitively coupled to a detector. We considered two kinds of non-equilibrium situations: (i) voltage biased QD (ii) thermal imbalance with different QD lead and detector temperatures. In both these cases, we showed that α can be reliably extracted at strong enough non-equilibrium ($V \gg T$ or $T_1 \gg T_0$).

We believe that our schemes can be easily implemented in existing experimental setups with minor modifications. Such an experimental detection of AOC effects would open the door towards the exploration of more exotic effects such as the quantum phase transitions discussed

in Ref. 5,6.

Acknowledgments

We gratefully acknowledge support from the European Research Council (ERC) under the European Union Horizon 2020 research and innovation programme under grant agreement No. 951541. ARO (W911NF-20-1-0013). Y.M. acknowledges support from ISF Grant No. 359/20 and 737/24. J.F. acknowledges support from the Natural Sciences and Engineering Research Council of Canada; the Canadian Institute for Advanced Research; the Max Planck-UBC-UTokyo Centre for Quantum Materials and the Canada First Research Excellence Fund, Quantum Materials and Future Technologies Program.

* sarathsankar@tauex.tau.ac.il

- ¹ P. W. Anderson, Phys. Rev. Lett. **18**, 1049 (1967).
- ² I. L. Aleiner, N. S. Wingreen, and Y. Meir, Phys. Rev. Lett. **79**, 3740 (1997).
- ³ S. Sankar, C. Bertrand, A. Georges, E. Sela, and Y. Meir, Phys. Rev. B **110**, 085133 (2024).
- ⁴ S. Sankar, M. Lotem, J. Folk, E. Sela, and Y. Meir, arXiv preprint arXiv:2503.03416 (2025).
- ⁵ M. Goldstein, R. Berkovits, and Y. Gefen, Phys. Rev. Lett. **104**, 226805 (2010).
- ⁶ Z. Ma, C. Han, Y. Meir, and E. Sela, Phys. Rev. Lett. **131**, 126502 (2023).
- ⁷ L. Borda, K. Vladár, and A. Zawadowski, Phys. Rev. B **75**, 125107 (2007).
- ⁸ V. Kashcheyevs, C. Karrasch, T. Hecht, A. Weichselbaum, V. Meden, and A. Schiller, Phys. Rev. Lett. **102**, 136805 (2009).
- ⁹ E. Buks, R. Schuster, M. Heiblum, D. Mahalu, and V. Umansky, Nature **391**, 871 (1998).
- ¹⁰ M. Avinun-Kalish, M. Heiblum, A. Silva, D. Mahalu, and V. Umansky, Phys. Rev. Lett. **92**, 156801 (2004).
- ¹¹ B. Küng, S. Gustavsson, T. Choi, I. Shorubalko, T. Ihn, S. Schön, F. Hassler, G. Blatter, and K. Ensslin, Phys. Rev. B **80**, 115315 (2009).
- ¹² D. Bischoff, M. Eich, O. Zilberberg, C. Rossler, T. Ihn, and K. Ensslin, Nano letters **15**, 6003 (2015).
- ¹³ M. S. Ferguson, L. C. Camenzind, C. Müller, D. E. F. Biesinger, C. P. Scheller, B. Braunecker, D. M. Zumbühl, and O. Zilberberg, Phys. Rev. Res. **5**, 023028 (2023).
- ¹⁴ X.-G. Wen, *Quantum Field Theory of Many-body Systems—from the Origin of Sound to an Origin of Light and Fermions* (Oxford University Press, 2003).
- ¹⁵ P. Nozierés and C. De Dominicis, Phys. Rev. **178**, 1097 (1969).
- ¹⁶ T.-K. Ng, Phys. Rev. B **54**, 5814 (1996).
- ¹⁷ B. Muzykantskii, N. d’Ambrumenil, and B. Braunecker, Phys. Rev. Lett. **91**, 266602 (2003).
- ¹⁸ D. Abanin and L. Levitov, Phys. Rev. Lett. **94**, 186803 (2005).
- ¹⁹ N. Hartman, C. Olsen, S. Lüscher, M. Samani, S. Fallahi, G. C. Gardner, M. Manfra, and J. Folk, Nature Physics **14**, 1083 (2018).
- ²⁰ T. Child, O. Sheekey, S. Lüscher, S. Fallahi, G. C. Gardner, M. Manfra, A. Mitchell, E. Sela, Y. Kleeorin, Y. Meir, et al., Phys. Rev. Lett. **129**, 227702 (2022).
- ²¹ C. Adam, H. Duprez, N. Lehmann, A. Yglesias, S. Cances, M. J. Ruckriegel, M. Masseroni, C. Tong, A. O. Denisov, W. W. Huang, et al., arXiv preprint arXiv:2412.18000 (2024).
- ²² N. Cooper and A. Stern, Phys. Rev. Lett. **102**, 176807 (2009).
- ²³ K. Yang and B. I. Halperin, Phys. Rev. B **79**, 115317 (2009).
- ²⁴ G. Viola, S. Das, E. Grosfeld, and A. Stern, Phys. Rev. Lett. **109**, 146801 (2012).
- ²⁵ G. Ben-Shach, C. R. Laumann, I. Neder, A. Yacoby, and B. I. Halperin, Phys. Rev. Lett. **110**, 106805 (2013).
- ²⁶ G. Ben-Shach, A. Haim, I. Appelbaum, Y. Oreg, A. Yacoby, and B. I. Halperin, Phys. Rev. B **91**, 045403 (2015).
- ²⁷ S. Smirnov, Phys. Rev. B **92**, 195312 (2015).
- ²⁸ E. Sela, Y. Oreg, S. Plugge, N. Hartman, S. Lüscher, and J. Folk, Phys. Rev. Lett. **123**, 147702 (2019).
- ²⁹ C.-Y. Hou, K. Shtengel, G. Refael, and P. M. Goldbart, New J. Phys. **14**, 105005 (2012).
- ³⁰ C. Han, Z. Iftikhar, Y. Kleeorin, A. Anthore, F. Pierre, Y. Meir, A. K. Mitchell, and E. Sela, Phys. Rev. Lett. **128**, 146803 (2022).
- ³¹ S. Sankar, E. Sela, and C. Han, Phys. Rev. Lett. **131**, 016601 (2023).